Design of a 2 × 2 Programmable Matrix of Silicon Photonic Switches Based on Mach-Zehnder Interferometer Structures Using the Thermo-Optic Effect

Ernesto Velazquez [a], Alessandro Fantoni [a, b], Paulo Lourenço [a, b]
[a]ISEL - Instituto Superior de Engenharia de Lisboa, Instituto Politecnico de Lisboa, Portugal.
[b]Center of Technology and Systems (CTS) and Associated Lab of Intelligent Systems (LASI), Caparica, Portugal.
a50267@alunos.isel.pt ernesto.velazquez@outlook.pt

2025 9th International Young Engineers Forum on Electrical and Computer Engineering (YEF-ECE) | 979-8-3315-0401-4/25/$31.00 ©2025 IEEE | DOI: 10.1109/YEF-ECE66503.2025.11117252

***Abstract* — The Mach-Zehnder Interferometer (MZI) has been extensively deploying in a variety of modern photonic circuits. With the integration of optical switches, this part serves as a fundamental element in the development of more sophisticated structures in the contemporary era of the photonics industry. In this work, we propose a basic design of a 2x2 programmable optical matrix using MZI interferometer's structure and the thermo-optical effect (TOE) as a control technique to obtain the change in the optical signal in the Bar, Cross, and Partial states, resulting in a thermally reconfigurable photonic integrated circuit (PIC). The forward-only waveguide network architecture, in which light flows through each element in only one direction, will be employed. Simulations tools as Synopsys Rsoft software will be used for simulation and results. The goal of this study is to analyse the design of a basic structure, which can be conceptualised as a block within a matrix or a more advanced solution for photonic applications, including, reconfigurable photonic networks, wavelength division multiplexing (WDM) and artificial neural networks.**

Keywords* — *Mach-Zehnder interferometer, photonic integrated circuit, thermo-optical effect, wavelength division multiplexing, photonic, optical switches, programmable optical matrix.

I. Introduction

PICs are the evolution of the photonic version of electronic Integrated Circuits (ICs) technology, also commonly known as Chips. As is well known, ICs are classified into two types depending on their functionality: Application-Specific Integrated Circuit (ASIC) which is designed and built for a specific application or purpose without being possible to modify or reprogram its functions and Field Programmable Gate Array (FPGA) which has as a determining factor its general use based on the use of Configurable Logic Blocks (CLB) and programmable connections, being possible to reprogram its functionalities depending on its resources. In technology, integrated circuits (ICs) and programmable circuits (PICs) share similarities in their construction, both designed on a dielectric base. Taking advantage of manufacturing compatibility with CMOS technology, PICs are commonly manufactured using silicon-on-insulator (SOI) technology. The layered construction of these circuits is achieved using advanced lithography techniques, a key process in the manufacture of photonic integrated circuits [1]. Although there are common features regarding the high-level design of PICs and FPGAs, the basic principles of operation are substantially different, due to the nature of operation and their physical characteristics, since PICs do not perform digital logic operations, but take advantage of the optical properties and different photonic effects to perform very high-speed analogue operations by acting on the spectral arameters such as phase, amplitude, frequency and polarisation of the optical signals in a controlled environment.

One of the functionalities of PIC architecture are the optical switches, which have as one of their principles the change of the light path without the use of moving parts, by controlling the variation of the refractive index by various effects such as the thermo-optical effect (TOE) [2, 3] , the electrooptic effect (EOE) [4, 5, 6] the acoustic-optic effect (AOE) [7, 8, 9] , and the magneto-optic effect (MOE) [10, 11, 12] as the most important. In this work we will select the TOE since this effect is generally applicable to all materials and its implementation as a control element is simple and effective. These can be easily designed using a variety of structures on a waveguide platform, commonly used in silicon on insulator (SOI), the most popular being microring resonators (MRR) [13, 14, 15], mach-zehnder interferometers (MZI) [16, 17, 18, 19] and multimode interferometer (MMI) [20, 21, 22].

MZI architecture aims to isolate a fraction of light using a defined structure, such as a longer path than the other fraction of light, or by using the effects to perform a phase shift. This operating principle is widely used as an optical modulator/demodulator. In [17], a 2x3 design is analyzed, and in [1], a 5x5 solution is analyzed. In both cases, the use of MZI depends on the solution proposed by the authors and the technological needs to be addressed. This work proposes a 2x2 optical matrix based on directional couplers using thermo-optic effect as a control technique, combined with an MZI structure as a modulator. This structure is useful for applications such as a state matrix, optical switch, and programmable modulator. By controlling these switches, various configurations can be achieved, such as Bar, Cross, and Partial states, with the aim of addressing the design and providing a solution that differs from the current literature. Using resistive heaters through the TOE effect, we will control the optical paths in the directional couplers. By increasing the temperature, the effective refractive index in the material will change, causing a variation in the modal propagation constant, so altering the interference pattern within the segment in the guide of interest, both for the coupler and for the interferometer.

II. Principles of Thermo-Optic Effect

The use of TOE in modulators and as control elements is very popular due to the simplicity of its construction, although it is not very efficient in applications that require high processing capacity, due to the time it takes to heat up the guide and cool down, as well as thermal dissipation in terms of

979-8-3315-0401-4/25/$31.00 ©2025 IEEE

efficiency. Despite its disadvantages, it is very useful in medical applications, such as biosensors and sensor control systems, as well as in other applications of interest, such as optical switches, lasers, tunable filters, and programmable arrays [23].

Devices that use the TOE to control phase shifting are also known as Thermo-optic phase shifter (TOPS), the phase variation is expressed as [3, 24, 25]:

$$\Delta n = \left(\frac{\partial n_{eff}}{\partial T}\right)\Delta T\,, \tag{1}$$

$$\Delta\phi = \frac{2\pi}{\lambda} L_{eff} \cdot \left(\frac{\partial n_{eff}}{\partial T}\right)\Delta T\,, \tag{2}$$

where λ is the wavelength in nm, L_{eff} is the effective heater length, Δn is the change in refractive index due to temperature, $\partial n_{eff}/\partial T$ is the is the effective thermo-optic coefficient of the waveguide, this value change by the geometry in the waveguide, not represent the value for the material, and ΔT, it is the variation of temperature at room, standardized at 300 K. Fig. 1 shows a representation of TOPS on silicon waveguide, in a) the heat flow generated by the resistive heater and in b) the variation of the refractive index due to the increase of the temperature by means of the conduction of the heater shown in a).

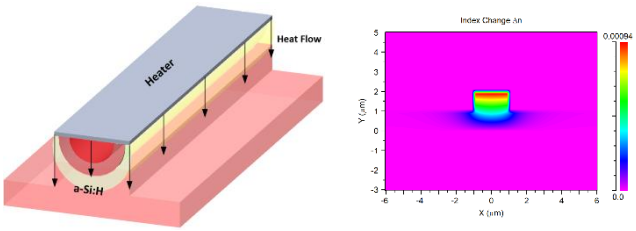

a) b)

Fig. 1. Representations of TOE on single silicon waveguide, a) single TOPS, b) termo-optic variations on Si waveguide

Thermal conductivity is the property that measures a material's ability to conduct heat, which is very useful when choosing which metal or material to use as a heater. In thin film, thermal conductivity is much lower than in materials with a larger volume $(mm)^3$ due to the dispersion of phonons at the interface with the substrate, thus reducing the efficiency of heat transport [26]. The thermal resistance of a plane wall is calculated using the following from [27]:

$$R_t = \frac{L}{kA}\,, \tag{3}$$

where k determined the thermal conductivity of the material, a high k value indicates that the material is a good thermal conductor. A determines the cross-sectional area to heat flow and L is the thickness of the layer. The electric resistance is given by:

$$R = \rho_e \frac{L}{A}\,, \tag{4}$$

also known as Ohm's law, where ρ_e represents the electrical resistivity of the material, and the voltage V is defined by:

$$V = \sqrt{P \cdot R}\,, \tag{5}$$

where P quantifies the electrical energy dissipated by the resistive microheater.This power changes the temperature in the waveguide, as stated in the equation 7, linking the thermal response of the system to the applied electrical input.

It is understood that phonons in a solid exhibit behavior analogous to those of particles in a gas with respect to energy transport. Consequently, the thermal conductivity in solids is characterized as the heat flow resulting from the motions and interactions of phonons. The thermal conductivity can be calculated by the following expression referred in [28]:

$$k = \frac{1}{3} C v \Lambda_{eff}\,, \tag{6}$$

where C represents the heat capacity per unit volume, v is the propagation speed of acoustic phonons and Λ_{eff} is the average distance phonons travel between scattering events, known as the effective mean free path. In terms of heat generation by heat dissipation (joule effect) through a resistive element the temperature variation is described by [3, 24] as:

$$\Delta T = \frac{\eta P}{C_p \rho L S}\,, \tag{7}$$

were, η represents the efficiency with which electrical power is used to generate the desired thermal change, P is the power dissipated by the resistive heating element, C_p corresponds to the specific heat capacity of the waveguide material, ρ determined the material density of the waveguide, and S denotes the cross-sectional area through which the thermal energy is distributed.

A. TOPS Basic Configurations

As it can be deduced, to transmit heat a heater is necessary in the SOI structure, the different configurations for the design of a PIC with TOPS have been analyzed, the most relevant ones are presented in this work [3, 18, 29]. In the Fig. 2 showing the main configurations for TOPS,

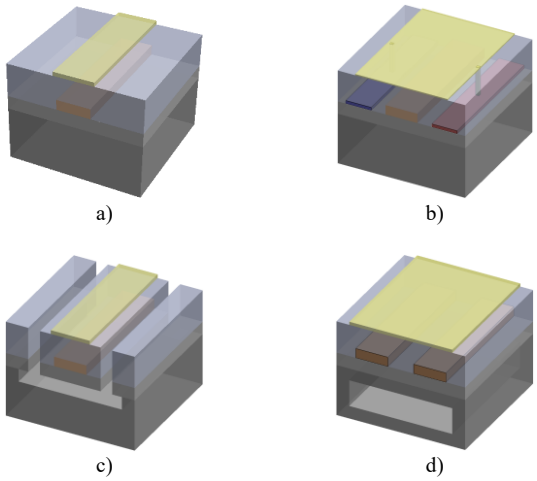

a) b)

c) d)

Fig.2. Representations of different basic TOPS configurations. a) waveguide and resistive heater on the top. b) waveguide and resistive heater on the top, with doped silicon heaters on both sides at symmetrical distance d c) waveguide and metal heater on the top with trench for air gap and substrate undercutting. d) multiple separate waveguides with a resistive heater on the top and trench for air gap and substrate undercutting.

B. Directional coupler

One of the applications of using TOPS, is that using this effect a directional coupler can be implemented, which is very useful and widely used in advanced applications, this coupler is often used with MZI and MMR, within the current technological solutions, rather than the phase variation of the signal the objective is to achieve the optical coupling between two waveguides close, this effect is known and widely used in ASIC solutions.

Coupled Mode Theory (CMT) defines how electromagnetic modes propagate and couple along the longitudinal z-axis due to the superposition of the fields by the physical properties of the guide and its design parameters such as length, width, height and angle. Several relevant papers have been published, highlighting the work of Hardy and Streifer in [30], where a generalized formulation of the CMT is proposed extending the classical orthogonal theory collected by Huang in [31], to the concept of non-orthogonal superposition, introducing terms of "self-coupling" and "cross-power", in addition the model quantifies the effect of phase mismatch Δβ, dispersion, losses or irregular geometries, being relevant in the performance of modulators and optical switches.

Numerous theoretical and experimental investigations have recently addressed their operation and design characteristics in [32, 19, 33, 34]. The proportion of optical power transferred from one waveguide to another in a directional coupler can be described by the following expressions [35]:

$$t^2 = \frac{P_{(Through)}}{P_{in}} = \cos^2(\kappa L) \ , \tag{8}$$

$$c^2 = \frac{P_{(Cross)}}{P_{in}} = \sin^2(\kappa L) \ , \tag{9}$$

$$t^2 + c^2 = 1 \, . \tag{10}$$

where t represents the power through coupling coefficient, corresponding to the fraction of input optical power that continues along the same waveguide (the "through" port), the coupler, c represents power cross coupling coefficient, indicating the fraction of power that is transferred to the adjacent waveguide (the "cross" port), Pin denotes the total power at the coupling input, $P_{Trhough}$ is the power remaining in the input waveguide, P_{cross} is the power transferred to the adjacent waveguide, L is the effective length of the coupler and κ is the coupling coefficient which is represented by:

$$\kappa = \frac{2h^2 q e^{-qs}}{\beta W (q^2 + h^2)} \ , \tag{11}$$

where W is the width of the waveguide channel, s represents the distance separating the waveguides as show in the Fig. 4, h and β are the propagation constants in the vertical and longitudinal directions respectively, and q is the attenuation (extinction coefficient) in the vertical direction. The full transfer of optical power from one waveguide to the other occurs at the coupling length L_c, which is calculated as:

$$L_c = \frac{\pi}{2\kappa} + \frac{m\pi}{\kappa} \ , \ m = 0,1,2.. \tag{12}$$

With the use of the directional actuator technique we can obtain one of the three states shown in Fig. 3. By means of TOPS it is possible to alter these states, which allows programmable control.

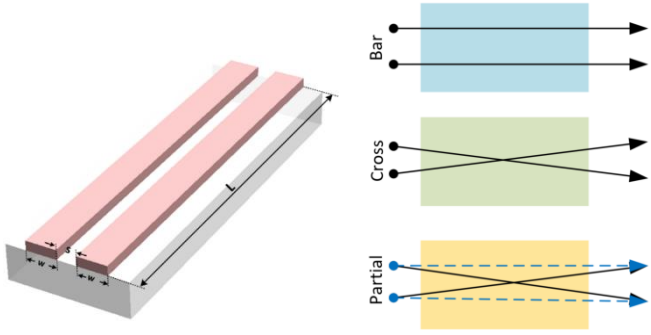

a) b)

Fig. 3. Directional Coupler, a) schematic representation of a directional coupler based on two parallel rectangular optical guides separated by a distance s, b) diferents controls states.

III. Basic Block Programable Directiona Coupler

A. Mach Zehnder Interferometer

The simplest way to implement an MZI interferometer is by using a Y-branches splitter/combiner, a waveguide structure as shown in Fig. 4 a), another other option is using a directional coupler as shown in b) or a combination of both.

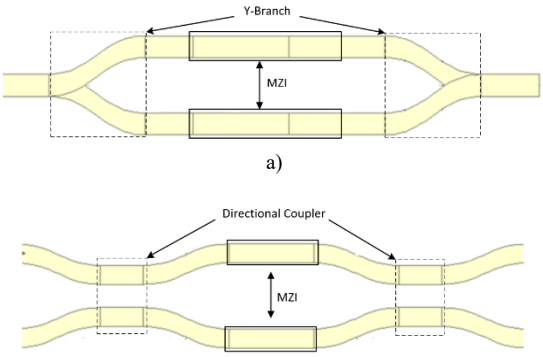

a)

b)

Fig. 4. Basics MZI structures a) Structure MZI whit directional coupler, b) whit Y-branches

In the solution using the Y-branch configurations, the *splitter* and *combiner* are connected by two optical waveguides whose lengths can be either identical or different, depending on the application and the modulation scheme adopted. The frequency of the modulated optical signal at the combiner's output is decided by the length difference between the two waveguide arms [23]. Depending on the technique used, and the variation in the refractive index in the segment, an output will be obtained for the same wavelength, which may be destructive or constructive depending on the phase variations in the paths between the guides, or the variations caused by the methods, in this case by the temperature in the MZI guide L1/L2 segment.

B. Simulation and Modelling Directional Coupler

For this project, we will analyze two structures at an initial temperature of 300 K. Whenever we talk about temperature variation it is referred to this value, which we will normalize, given the parameters of the simulation software and its algorithm, the first 3dB 50/50 partial state coupler and a cross coupler. The goal of these designs is to change their state at T_{300K} through temperature control. Later, we will analyze each

of these solutions in more detail, and finally, they will be integrated into the proposed solution outlined in the introduction of this work.

The simulations were implemented using RSoft software, specifically the BeamPROP algorithm. This numerical algorithm is particularly useful for analyzing wave propagation in optical waveguiding structures. The approach involves allowing the input optical beam to propagate over a short segment in a uniform medium, followed by a correction stage that accounts for the refractive index variations encountered along this segment [36].

In the waveguide design, width and height values of 0.5 µm were specified to achieve a single-mode channel, in conjunction with material characteristics. In Fig. 5, propagation modes were calculated, yielding the following results for the fundamental TE/TM modes.

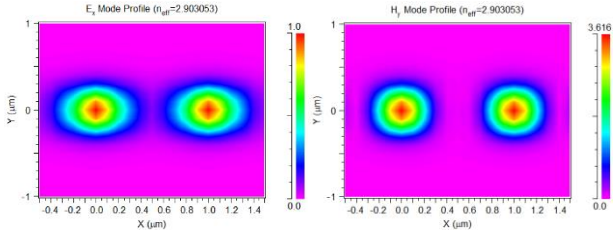

Fig. 5: TE/TM mode profile of strip waveguide

C. Thermo-optic directional Coupler 3dB.

To calculate the coupling coefficient κ and the value of β, to determine the coefficients t and c, Mercantill's algorithm was recreated in Python, which was also used to determine n_{eff}, according to the dimensions of the rectangular guide. The code will be available in Github [37] . In Fig. 6, the simulation for $t^2 = c^2 = 0.5$ at an electrode temperature of T=0 can be seen.

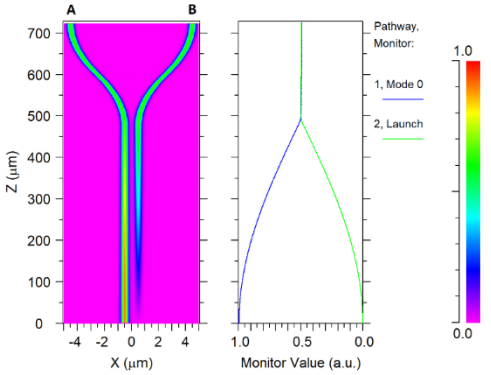

Fig. 6. Simulation of the coupler for t^2=c^2= 0.5, ΔT =0K

As shown in Fig. 7, as the temperature increases, the optical power fraction is more confined in A ($P_{(Through)}$), starting from a default 3dB coupling configuration for ΔT_{300K} = 0K. It was analyzed for temperatures up to 400K, given that at 50K, total confinement in A can be seen, as shown in Fig. 8. For higher values, guide B also received more temperature, and a chain heating effect occurred, which was not desired. To obtain better results, control at the lowest possible temperature is looked for.

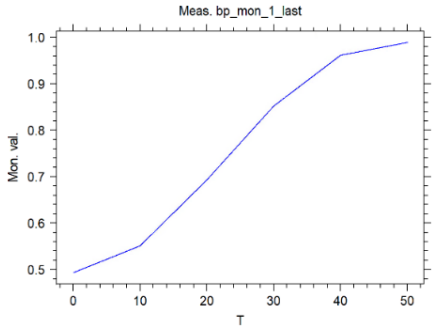

Fig. 7. Simulation of the directional coupler 3dB at, ΔT=50K

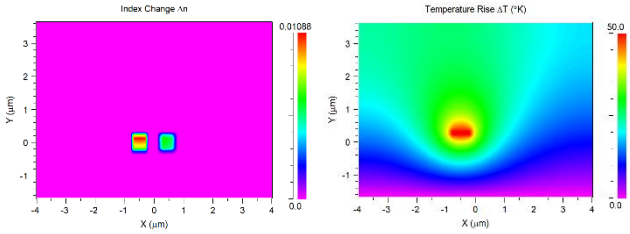

a) b)

Fig. 8. Thermo-Optic effect in Si waveguide, a) variation in refractive index due to the TOE effect , b) heat radiation map for the heater at 350K

D. Thermo-optic directional coupler cross configuration

In this configuration as shown in Fig. 9, the value of s was calculated, which would provide a total cross at a temperature of 300K. By controlling the temperature, the optical power values at the output were controlled in the same way as in the earlier configuration, in Fig. 10 we can see the variation at ΔT=50K.

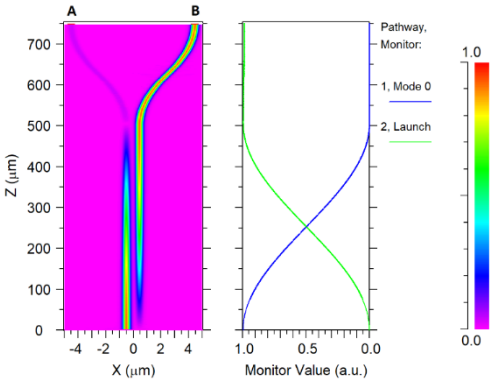

Fig. 9. Simulation of the coupler cross configuration, at ΔT=0K.

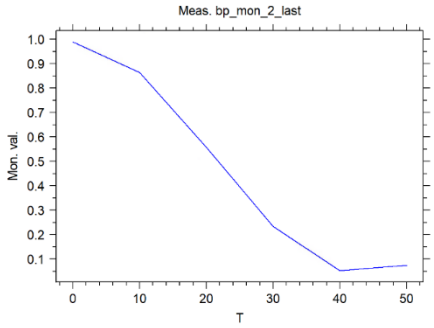

Fig. 10. Simulation of the directional coupler cross at, ΔT=50K

In this analysis, we were unable to achieve a 100% power transfer value at the output. The closest value was reached at 40K, with a value of $P_{(Through)}$ = 0.95

IV. Proposal for a 2x2 Programmable Matrix Using the Thermo-Optic Effect

As shown in Fig. 11, the proposed design is based on the MZI interferometer model shown in Fig. 4, which consists of a configurable coupler and a phase shifter. A second stage has been added to this design as shown in block B.

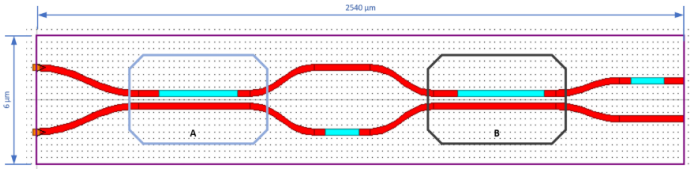

Fig. 11. 2x2 Programmable Matrix – MZI

From the analysis performed in table 1, which shows a better use of the combinations of temperature vs. the percentage of power of the outputs in each case, referent the values obtained in the Fig. 7 and 10. This will help us later present the state table of the results obtained in the simulations for one and two optical light sources at power=1, phase=0.

Table I. Selected Results from Fig.7 and Fig.10

	Signal in A		Signal in B	
$\Delta T(K)$	$P_{(Through)}$	$P_{(Cross)}$	$P_{(Through)}$	$P_{(Cross)}$
0	50	50	0	100
40	95	5	95	5
50	100	0	92	8

The tests conducted were considered for 0 and 50 K, divided into two parts. The first part, which we will address below, involves a single light source, and the second part involves the behavior with two light sources, both at 1550 nm. As shown in Fig. 12, the output for T=0 is shown, and in Fig. 13, the output for T=50K is shown.

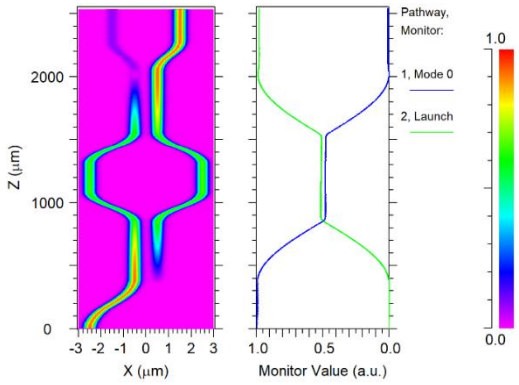

Fig. 12. Simulation T=0

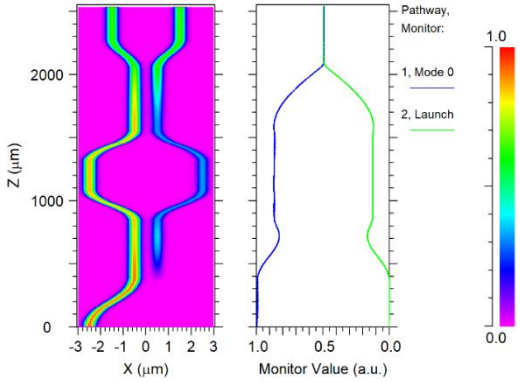

Fig. 13. Simulation T=50K

We performed the same analysis for two light sources. From the results obtained, we have the following table:

Table II. Results Obtained for a Single Light Source

	Signal in A		Signal in B	
$\Delta T(K)$	$P_{(Through)}$	$P_{(Cross)}$	$\Delta T(K)$	$P_{(Through)}$
0	50	50	0	100
50	90	10	50	50

Table III. Results Obtained for Two Light Sources

	Signal in A		Signal in B	
$\Delta T(K)$	$P_{(Through)}$	$P_{(Cross)}$	$\Delta T(K)$	$P_{(Through)}$
0	50	50	50	50
50	50	50	0	100

Fig. 14 shows the behavior of the couplers when a light source is introduced through both inputs at the same time. It can be observed that in both cases, for the different configurations performed, there is a mixture between the output signals, which demonstrates that these couplers are suitable for working with one signal at a time, although in DWDM systems they normally work depending on the input signal, provided that the carrier frequencies are not the same.

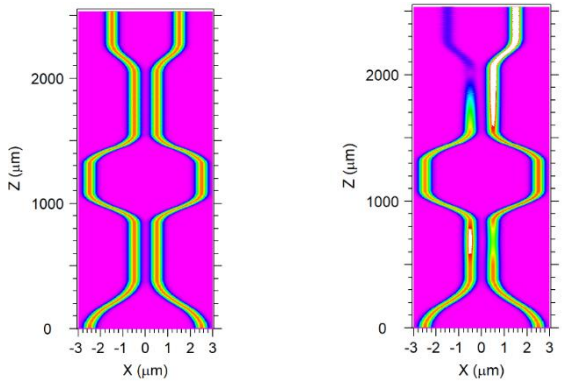

a) b)

Fig. 14. Simulation of Two Light Sources a) for ΔT=0, b) for ΔT=50K

Conclusions

This work proved that the use of the thermo-optic effect helps the creation of more complex matrices from simple structures. The successful design of a programmable matrix employed directional couplers and the MZI interferometer as a modulator element, with experimental verification of the results.

ACKNOWLEDGMENTS

This research was supported by Portuguese national funds provided by the Portuguese FCT program, Center of Technology and Systems, (CTS) UIDB/00066/2020/UIDP/00066/2020, and by IPL projects \IPL/IDI&CA2024/OPAPIC2D ISEL e IPL/IDI&CA2024/REFINDEX_ISEL.

REFERENCES

[1] W. Bogaerts, D. Pérez, J. Capmany, D. A. B. Miller, J. Poon, D. Englund and F. M. &. A. Melloni, "Programmable photonic circuits," *Nature,* no. 586, pp. 207-216, 2020.

[2] F. G. D. Corte, M. E. Montefusco, L. Moretti, I. Rendina and a. G. Cocorullo, "Temperature dependence analysis of the thermo-optic effect in silicon by single and double oscillator models," *Journal Of Applied Physics,* vol. 88, no. 12, pp. 7115-7119, 2000.

[3] S. Liu, J. Feng, H. Z. Ye Tian, L. Jin, B. Ouyang and J. Z. &. J. Guo, "Thermo-optic phase shifters based on silicon-on-insulator platform: state-of-the-art and a review," *Frontiers of Optoelectronics ,* vol. 15, no. 9, 2022.

[4] J. V. Campenhout, W. M. J. Green and a. Y. A. Vlasov, "Design of a digital, ultra-broadband electro-optic switch for reconfigurable optical networks-on-chip," *Optical Express,* vol. 17, no. 23, pp. 793-808, 2009.

[5] K. Powell, L. Li, A. Shams-Ansari, J. Wang, D. Meng, N. Sinclair, J. Deng, M. Lončar and a. X. Yi, "Integrated silicon carbide electro-optic modulator," *Nature Communications,* vol. 13, no. 1851, 2022.

[6] B. Zabelich, E. Nitiss, A. Stroganov and a. C.-S. Brès, "Linear Electro-optic Effect in Silicon Nitride Waveguides Enabled by Electric-Field Poling," *ACS Photonics,* vol. 9, no. 10, pp. 3374-3383, 2022.

[7] T. A. Birks, P. S. J. Russell and a. D. O. Culverhouse, "The acousto-optic effect in single-mode fiber tapers and couplers," *Journal of Lightwave Technology ,* vol. 14, no. 11, pp. 2519-2529, 2022.

[8] C. A. F. Marques, L. Bilro, L. Kahn, R. A. Oliveira, D. J. Webb and a. R. N. Nogueira, "Acousto-Optic Effect in Microstructured Polymer Fiber Bragg Gratings: Simulation and Experimental Overview," *Journal of Lightwave Technology,* vol. 31, no. 10, pp. 1551-1558, 2013.

[9] B. Pan, H. Liu, Y. Huang, Z. Yu, H. Li, Y. Shi, L. Liu and a. D. Dai, "Perspective on Lithium-Niobate-on-Insulator Photonics Utilizing the Electro-optic and Acousto-optic Effects," *ACS Photonics,* vol. 10, no. 7, pp. 1999-2439, 2023.

[10] T. Haider, " Review of Magneto-Optic Effects and Its Application," *International Journal of Electromagnetics and Applications,* vol. 7, no. 1, pp. 17-24, 2017.

[11] H. Chen, M. Ye, N. Zou, B.-L. Gu, Y. Xu and W. Duan, "Basic formulation and first-principles implementation of nonlinear magneto-optical effects," *APS Physical Review Journals,* vol. 105, no. 14, pp. 75-123, 2022.

[12] M. J. Frieser, "A survey of magneto optic effects," *IEEE Transactions on Magnetics,* vol. 4, pp. 152-161, 1986.

[13] W. Bogaerts, P. D. Heyn, T. V. Vaerenbergh, K. D. Vos, S. K. Selvaraja, T. Claes, P. Dumon, P. Bienstman, D. V. Thourhout and R. Baets, "Silicon microring resonators," *Laser & Photonic Reviews,* vol. 6, no. 1, pp. 47-73, 2012.

[14] Y. R. Bawankar and A. Singh, "Microring Resonators Based Applications in Silicon Photonics - A Review," in *5th Conference on Information and Communication Technology (CICT)*, Kurnool, India, 2021.

[15] "Photonic Neural Networks Based on Integrated Silicon Microresonators," *Intelligent Computing,* vol. 3, no. 67, 2024.

[16] X. Xu, Y. Yin, C. Sun, J. Li, H. Lin, B. Tang, P. Zhang, L. Li and D. Zhang, "Polycrystalline silicon 2 × 2 Mach-Zehnder interferometer optical switch," *Optics Express,* vol. 31, no. 18, pp. 29695-29702, 2023.

[17] S. Kaur, M. L. Singh, Priyanka and a. a. M. Singh, "Design of electro optic Mach–Zehnder interferometer based all optical binary half adder and half subtractor," *Optical and Quantum Electronics,* vol. 54, no. 341, 2022.

[18] Y. Xie, Y. Shi, L. Liu, J. Wang, R. Priti, G. Zhang, O. Liboiron-Ladouceur and D. Dai, "Thermally-Reconfigurable Silicon Photonic Devices and Circuits," *IEEE Journal of Selected Topics in Quantum Electronics,* vol. 26, no. 5, pp. 1-20, 2020.

[19] S. Chen, Y. Shi, S. He and D. Dai, "Low-loss and broadband 2 × 2 silicon thermo-optic Mach–Zehnder switch with bent directional couplers," *Optics Letters,* vol. 41, no. 4, pp. 836-839, 2016.

[20] N. Xie, T. Hashimoto and K. Utaka, "Very low power operation of compact MMI polymer thermooptic switch," *IEEE Photonic Technology,* vol. 21, no. 18, pp. 1335-1337, 2009.

[21] F. Duan, K. Chen, D. Chen and Y. Yu, "Low-power and high-speed 2 × 2 thermo-optic MMI-MZI switch with suspended phase arms and heater-on-slab structure," *Optics Letters,* vol. 46, no. 2, pp. 234-237, 2021.

[22] S.-H. Kim, J.-B. You, H.-W. Rhee, D. E. Yoo, D.-W. Lee and K. Yu, "High-Performance Silicon MMI Switch Based on Thermo-Optic Control of Interference Modes," *IEEE Photonics Technology Letters,* vol. 30, no. 16, pp. 1427 - 1430, 2018.

[23] H. Oulachgar, L. Chrostowski and B. R, "Silicon Photonics Design, Fabrication and Data Analysis," Researchgate, The University of British Columbia, Canada, 2015.

[24] D. Coenen, M. Kim, H. Oprins, J. V. Campenhout and I. D. Wolf, "A Critical Analysis of the Thermo-Optic Time Constant in Si Photonic Devices," *Photonics,* vol. 11, no. 7, p. 603, 26 6 2024.

[25] N. C. Harris, "Efficient, compact and low loss thermo-optic phase shifter in silicon," *Optics Express,* vol. 22, no. 9, pp. 10487-10493, 2014.

[26] M. H. Seungjae Moon, M. Lee and C. P. Grigoropoulos, "Thermal conductivity of amorphous silicon thin films," *International Journal of Heat and Mass Transfer,* vol. 45, no. 12, pp. 2439-2447, 2002.

[27] K. Alaili, J. O. Miranda and Y. Ezzahri, "Effective interface thermal resistance and thermal conductivity of dielectric nanolayers," *International Journal of Thermal Sciences,* vol. Volume 131, pp. 40-47, 2018.

[28] G. W. Xingli Zhang, "Effect of Strain on Thermal Conductivity of Si Thin Films," *Journal of Nanomaterials,* vol. Volume 2016, 2016.

[29] H. Sun, Q. Qiao, Q. Guan and G. Zhou, "Silicon Photonic Phase Shifters and Their Applications: A Review," *Micromachines,* vol. 13, no. 9, 2022.

[30] A. Hardy and a. W. Streifer, "Coupled Mode Theory of Parallel Waveguides," *Journal of lightwave technology,* vol. 3, no. 5, pp. 1135-1146, 1985.

[31] W.-P. Huang, "Coupled-mode theory for optical waveguides: an overview," *Journal of the Optical Society of America,* vol. 11, no. 3, pp. 963-983, 1994.

[32] Q. Xu, K. Xie, J. Tang and J. Ping, "Directional coupler design based on coupled cavity waveguides in photonic crystals," *Optik,* vol. 122, no. 13, pp. 1132-1135, 2009.

[33] M. Hamidah and a. R. W. Purnamaningsih, "An S-bend based optical directional coupler using GaN semiconductor," in *IEEE International Conference on Innovative Research and Development (ICIRD).*, Jakarta, Indonesia, 2019.

[34] H. Sattari, A. Y. Takabayashi, Y. Zhang, P. Verheyen, W. Bogaerts and N. Quack, "Compact broadband suspended silicon photonic directional coupler," *Optics Letters,* vol. 45, no. 11, pp. 2997-3000, 2020.

[35] Z. Lu, H. Yun, Y. Wang, Z. Chen, F. Zhang, N. A. F. Jaeger and L. Chrostowski, "Broadband silicon photonic directional coupler using asymmetric-waveguide based phase control," *Optics Express,* vol. 23, no. 3, pp. 3795-3808, 2015.

[36] J. Piprek, Handbook of Optoelectronic Device Modeling and Simulation Fundamentals, Materials, Nanostructures, LEDs, and Amplifiers, Boca Raton, Florida, USA: CRC Press , 2018.

[37] E. Velazquez, "Github," Github, 06 06 2025. [Online]. Available: https://github.com/evelazq3z/Marcatelli.git.